Output Voltage Correction for a Voltage Source Type Inverter of an Induction Motor Drive

Tetsuma Hoshino, *Member, IEEE*, and Jun-ichi Itoh, *Member, IEEE*

***Abstract*—A proposed voltage error correction method that uses a disturbance observer for various types of induction motor control was evaluated. The features of the proposed control method are: 1) control parameters are easily determined according to the motor model and the parameter sensitivity is robust, and 2) the proposed method can be applied for field-oriented vector control, speed sensor-less vector control, and *V/f* control of the induction motor by modification of a back electromotive force compensation term in the observer. The disturbance observer is designed to have fast response that is ten times faster than the current controller for vector control. The voltage error is efficiently corrected using the proposed method, and the current distortion can be reduced by approximately 1/3. The proposed method is validated on the basis of experimental results.**

***Index Terms*—DC–AC power conversion, induction motor drive, observers.**

NOMENCLATURE

p	Differential operator *d*/*dt*.
f_s	Switching frequency.
i_u	Output current of the leg.
i_1	Motor current of primary side.
$G_{\mathrm{ACR}}(s)$	Transfer function of automatic current regulator (ACR).
$G_{\mathrm{LPF}}(s)$	Transfer function of low-pass filter in the disturbance observer.
$G_{\mathrm{Motor}}(s)$	Transfer function of motor.
K_{ACR}	ACR proportional gain.
K_{FF}	Compensation gain.
L_m	Magnetizing inductance.
L_σ	Equivalent leakage inductance.
R_1	Primary resistance.
R_2	Secondary resistance.
T_d	Dead-time period.
T_f, T_s	Time constant of the observer.
V_{dc}	DC-link voltage.
V_{ON}	Saturation voltage of the switching device.
V_1	Motor voltage of primary side.
V_1^*	Command voltage for disturbance observer.
V_1^{**}	Command voltage for inverter.
ΔV	Disturbance voltage.
$\overline{\Delta V}$	Average disturbance voltage.
$\Delta \hat{V}$	Estimated error correction voltage.
$\hat{V}_{\mathrm{EMF}}$	Estimated speed electromotive force (EMF).
ϕ_2	Motor flux of secondary side.
ω_m	Motor speed in electric angular frequency.
ω_1	Primary-side angular frequency.
Subscripts	
C	Controller quantity.
d, q	d-and q-axes quantity.

Manuscript received December 9, 2009; revised February 5, 2010 and April 3, 2010; accepted April 9, 2010. Date of current version September 17, 2010. Recommended for publication by Associate Editor J. O. Ojo. This paper was presented at the IEEE Sixth International Power Electronics and Motion Control Conference, Wuhan, China, May 2009.

The authors are with Nagaoka University of Technology, Nagaoka 940-2188, Japan (e-mail: tetsuma@stn.nagaokaut.ac.jp; itoh@vos.nagaokaut.ac.jp).

Digital Object Identifier 10.1109/TPEL.2010.2049031

I. INTRODUCTION

THE output voltage of a power converter requires high accuracy to achieve high-performance operation of a motor drive, especially around the low-speed region. However, output voltage errors can be generated for two reasons. The first is the influence of a dead-time period. All voltage source type inverters require a dead time to prevent a short-circuit current in power devices. However, the dead time results in output voltage errors and significant distortion of the current waveform around the zero crossing point of the current. The second reason is the saturation voltage of a power device. The saturation voltage depends on the temperature and collector current of the power devices; therefore, the saturation voltage is varied.

In order to perform high-starting torque, low-speed ripple, low-torque ripple, and high-accuracy torque, correction of the output voltage error is a very important issue. In particular, when an induction motor drive operates without a speed sensor such as *V/f* control and sensor-less vector control, the output voltage error cannot be neglected in the low-voltage output range, such as at low speed.

Various voltage compensation methods have been previously proposed [1]–[10]. The most common method to compensate the dead time is the addition of the correction voltage to the output voltage command, according to the polarity of the current. If delay of the polarity detection or mismatching of the correction voltage occurs during the correction process, then a large distortion of the current waveform and a large torque ripple are generated. Polarity detection of the load current is particularly difficult in the low-speed region, because the transition of the polarity is very slow. In any case, it is difficult to compensate the voltage error using the saturation voltage of the power device, due to its nonlinear characteristics. It should be noted that the saturation voltage of the device is also a cause of the voltage error. Therefore, the dead-time elimination method is not sufficient for elimination of the voltage error [11]–[16].

On the other hand, a voltage error correction method that uses a disturbance observer has been proposed for vector-controlled systems [1], [9]. Compensation by a disturbance

observer is useful, because the disturbance observer can estimate the amount of voltage error, consisting of the saturation voltage of switching devices and the dead-time voltage error. In the method reported in [1], the disturbance observers decide only the compensation value. The output voltage correction is then implemented by adding the compensation value to the output voltage command according to the polarity of the load current, as with the conventional method. Therefore, it is difficult to solve the mismatch problem of the current polarity detection in the low-speed region using this method. For industrial products such as general purpose inverters, in order to compensate the voltage error by current polarity detection, the compensation value is adjusted at around the zero crossing point. This adjustment is very complex, because the voltage error characteristics are nonlinear. There have been some discussions regarding the voltage error correction without current polarity detection for induction motor drive applications. For example, support vector regression (SVR) algorithm has been proposed to correct the voltage error [12]. However SVR algorithm requires many memories for on-line voltage error estimation. On the other hand, the direct estimation of the voltage error using a disturbance observer was proposed for a permanent magnetic synchronous motor (PMSM) drive [9]. However, induction motors are widely used for various applications in comparison with the PM motor drive systems. The voltage error correction for an induction motor is still more important. There is a paper using a disturbance observer to correct voltage error for field-oriented vector control of an induction motor drive [17]. However, there has been no report of using a disturbance observer to correct voltage error for *V/f* control method, which is the most common method for adjustable speed drive.

We propose a voltage error correction method that uses a disturbance observer without current polarity detection. There are two main advantages of the proposed method. The first is that the control parameters can be easily determined according to the motor model, and the parameter sensitivity is robust. Even if the dead-time values changed, the proposed method can estimate the voltage error at on-line without parameter tuning. That is, the proposed method does not require parameter adjustment according to the load current, temperature, and dead time. The second advantage is that the proposed method can be applied to various control methods on the induction motor by only modification of a back EMF compensation term in the observer. The fundamental principle of the proposed compensation method is first described. Variation of the proposed method applied to sensor-less vector control and *V/f* control is then described. Lastly, experimental verifications are implemented on each control.

II. Principles of the Disturbance Observer for Voltage Error Correction

A. Problems With Conventional Compensation

Fig. 1(a) shows a circuit diagram of a voltage-source inverter, and Fig. 1(b) shows the voltage error behavior during a dead-time period. The voltage error is mainly caused by the dead-time period. The dead-time period T_d, when both switches are off, is

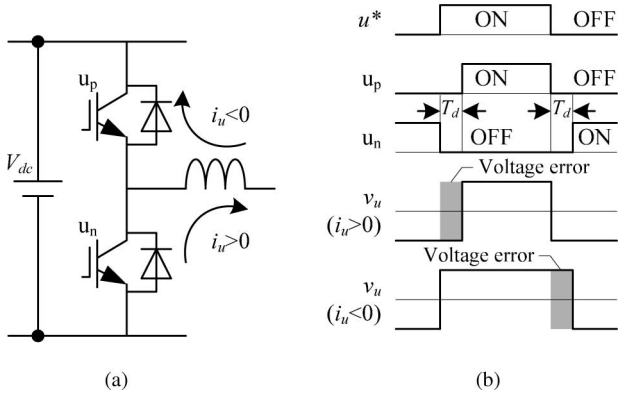

Fig. 1. Inverter leg circuit diagram and the relationship between the reference pulse and voltage error. (a) Inverter leg. (b) Relationship between the reference pulse and voltage error.

added at the transition of gate pulses u_p and u_n in order to avoid the short circuit between the upper and lower arms. An ideal inverter can set the dead time to zero; however, a real inverter must assign some dead-time period, because the actual switching device has a delay and dispersion of the switching characteristics. The voltage error is then caused from the conduction of the free-wheeling diode (FWD) during the dead-time period.

The voltage error during the dead-time period depends on the direction of the flowing current. When the direction of the output current from the leg to load is positive, the current in the leg flows through the FWD of the lower arm during the dead-time period. Thus, the output voltage is decreased by the dead-time period. On the other hand, when the output current direction is negative, the current in the leg flows through the FWD of the upper arm, and the output voltage is increased. The value of the voltage error depends on the dead-time period and the dc-link voltage, as shown in Fig. 1. The voltage error is calculated using (1).

$$\Delta V = -f_s T_d V_{\rm dc} \mathrm{sign}(i_u) \tag{1}$$

where sign(x) is a sign function. If $x > 0$ then sign(x) $= 1$, if $x < 0$ then sign(x) $= -1$, and if $x = 0$ then sign(x) $= 0$.

It should be noted that the magnitude of the voltage error is not dependent on the amplitude of the output voltage and the output current. Therefore, when the output voltage is small, such as during low-speed operation, the effect of the dead time is strong, because the ratio of the voltage error to output voltage becomes larger.

The voltage error is also derived from the saturation voltage $V_{\rm ON}$ of the switching device. When the output current direction of the leg is positive, the current in the leg does not flow through the switching device of the upper arm during the dead-time period. Thus, the output voltage is decreased by the saturation voltage of the device. On the other hand, when the output current direction is negative, the current in the leg flows through the device of the lower arm, and thus the output voltage is increased. The voltage error, which is dependent on the saturation voltage of the switching device, is calculated using (2).

$$\Delta V = -\left(1 - f_s T_d\right) V_{\rm ON} \mathrm{sign}(i_u). \tag{2}$$

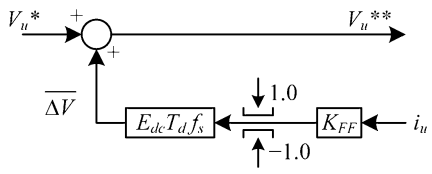

Fig. 2. Conventional voltage error correction method corresponding to the direction of the motor current.

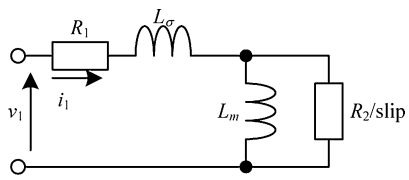

Fig. 3. Equivalent circuit of an induction motor.

Fig. 2 shows a control block diagram of practical voltage error correction according to the current polarity. The error correction voltage is calculated from $K_{FF}i_u$ limited to -1 and 1, where K_{FF} compensates the gain to maintain linearity at the zero-crossing point and prevent hunting. In order to achieve precise correction, the conventional method requires tuning of the gain K_{FF} for each converter. A practical inverter determines the voltage error differently from (1), because the output voltage is changed slowly by the junction capacitance of the switching device when the load current is around the zero-crossing point. In order to correct the voltage error precisely, an edge of the correction voltage is dulled by the gain K_{FF} at around the zero-crossing of the current waveform. The optimum value of the gain K_{FF} depends on the characteristics of each switching device; therefore, the tuning operation for each converter is a significant problem due to the long work time of practical inverters such as general-purpose inverters. In addition, the compensation value $f_sT_dV_{\rm dc}$ must also be adjusted according to the voltage saturation and switching characteristics of the power device.

B. Dead-Time Correction Method Using Disturbance Observers

A dead-time compensation method is proposed using a disturbance observer. The voltage error estimation uses the relationship between the motor voltage v_1 and current i_1 on a rotational frame, which is obtained using (3). Consequently, the tuning used for the conventional method will not be discussed here.

$$\begin{bmatrix} v_{1d} \\ v_{1q} \\ 0 \\ 0 \end{bmatrix} = \begin{bmatrix} R_1+pL_\sigma & -\omega_1 L_\sigma & p & -\omega_1 \\ \omega_1 L_\sigma & R_1+pL_\sigma & \omega_1 & p \\ -R_2 & 0 & \dfrac{R_2}{L_m}+p & -\omega_1+\omega_m \\ 0 & -R_2 & \omega_1-\omega_m & \dfrac{R_2}{L_m}+p \end{bmatrix} \times \begin{bmatrix} i_{1d} \\ i_{1d} \\ \phi_{2d} \\ \phi_{2q} \end{bmatrix}. \tag{3}$$

Fig. 3 shows the equivalent circuit of an induction motor on a *d–q* rotating frame. The secondary leakage inductance is converted into that of the primary side. The dead-time voltage error is estimated from the output current. From (3), when the *d*-axis corresponds to the vector of the secondary flux ϕ_2, the primary-side voltage v_1 is calculated using (4), because

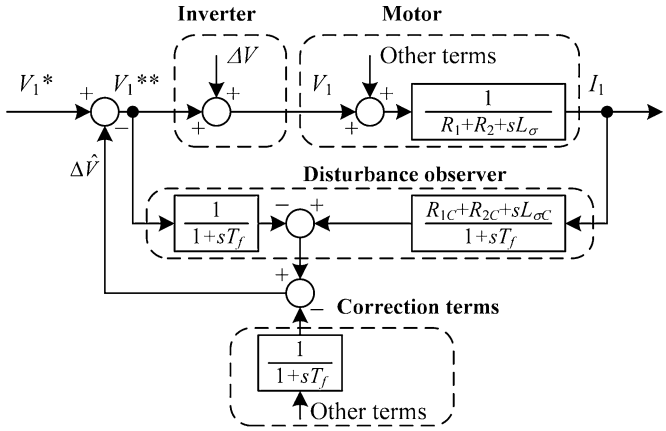

Fig. 4. Block diagram of the voltage error correction method using a disturbance observer.

the *q*-axis component ϕ_{2q} is equal to zero.

$$\begin{aligned} v_{1d} &= (R_1+R_2+pL_\sigma)\, i_{1d} - \omega_1 L_\sigma i_{1q} - \left(\frac{R_2}{L_m}\right)\phi_{2d} \\ v_{1q} &= (R_1+R_2+pL_\sigma)\, i_{1q} + \omega_1 L_\sigma i_{1d} + \omega_m \phi_{2d}. \end{aligned} \tag{4}$$

Fig. 4 shows a block diagram for the vector control method, using the proposed voltage error correction method. The disturbance observers calculate the difference between the command voltage V_1^{**} and the actual output voltage V_1 of the inverter, and estimates the disturbance voltage ΔV. The voltage error of the inverter becomes the disturbance of the voltage controller. The estimated voltage error is added to the voltage command as the error correction voltage $\Delta\hat{V}$, which is calculated using (5) derived from (4).

$$\begin{aligned} \Delta\hat{v}_d &= \frac{1}{1+sT_f}\left\{ (R_{1C}+R_{2C}+pL_{\sigma C})\, i_{1d} - \omega_1 L_\sigma i_{1q} - \left(\frac{R_2}{L_m}\right)\phi_{2d} - v_{1d}^{**} \right\} \\ \Delta\hat{v}_q &= \frac{1}{1+sT_f}\left\{ (R_{1C}+R_{2C}+pL_{\sigma C})\, i_{1q} + \omega_1 L_\sigma i_{1d} + \omega_m \phi_{2d} - v_{1q}^{**} \right\}. \end{aligned} \tag{5}$$

Bandwidth of the disturbance observer is determined by the time constant of the observer T_f. So T_f should be set as fast as possible, with consideration of the time delay of the feedback loop in order to neglect discretization effect such as phase lag.

The method proposed in Fig. 4 corrects only the first term on the right side of (5), which is the back EMF of the *RL*. The second and third terms in (5) are in proportion to the angular frequency of the primary and secondary sides, respectively. The second and third terms are referred to as the cross term and

speed EMF term, respectively. In the low-speed region, these terms can be neglected, because they are much smaller than the first term. The proposed method has good compensation performance in the low-speed region for each control method of the induction motor drive operation. However, the cross term and the speed EMF term interfere with the control performance in the middle- and high-speed regions. Therefore, the key point of applying the proposed method to various control methods is the implementation of these terms for correction according to the features of the control methods. In particular, calculation of the speed EMF term is important for the proposed method.

When the disturbance observer is combined with the ACR for voltage error correction, the transfer function of the proposed method from disturbance voltage ΔV to motor voltage V_1 is derived as

$$\frac{V_1}{\Delta V} = \frac{-(1 - G_{\mathrm{LPF}}(s))}{1 + G_{\mathrm{ACR}}(s)G_{\mathrm{Motor}}(s)}. \tag{6}$$

On the other hand, the transfer function of ACR from the disturbance voltage ΔV to the motor voltage V_1 is

$$\frac{V_1}{\Delta V} = \frac{-1}{1 + G_{\mathrm{ACR}}(s)G_{\mathrm{Motor}}(s)}. \tag{7}$$

That is, the transfer function from the disturbance voltage ΔV to the motor voltage V_1 does not equal regardless of the parameters in ACR. Then the slope of the magnitude characteristic in bode diagram at low frequency of the proposed method is different from that of ACR. The slope of the proposed method is -40 dB/dec, which is larger than -20 dB/dec of ACR.

Nonlinear voltage error is corrected by the disturbance observers in the proposed method. However, the voltage error correction in the overmodulation region cannot be corrected, because there is no margin to correct output voltage. The correction in the overmodulation region will be considered in future works.

An internal model control (IMC) method can estimate the output signal of plant, using an inverse model of the plant such as an induction motor. However, the IMC only estimates disturbance on the output side of the plant [18]. In this paper, the output signal of the plant is the input current of the motor. Therefore, the IMC is not suitable to use voltage error correction, because IMC does not estimate disturbance voltage of the input side.

III. Compensation Terms for Each Control Methods

A. Compensation Term for Field-Oriented Vector Control Method

Fig. 5 shows a block diagram of the proposed method applied to the field-oriented vector control method. In this control method, the cross term and speed EMF term in (5) are compensated by the feedforward control, because all parameters in this control method are known and the secondary angular frequency is known from the speed sensor. The disturbance observer is attached to the *d*-and *q*-axes.

The proposed method can also be applied to a sensor-less field-oriented vector control method. However, the speed sensorless control method should use an estimated motor speed instead

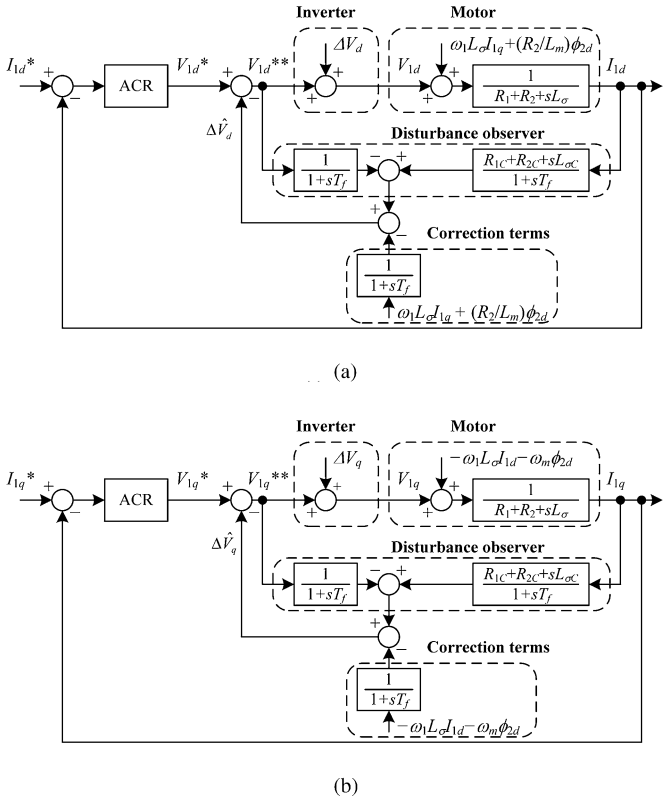

Fig. 5. Block diagrams of the voltage error correction method, using field-oriented vector control. (a) *d*-axis. (b) *q*-axis.

of an actual value ω_m for the speed EMF compensation. It should be noted that the voltage sensor for sensor-less vector control is not used for voltage error correction. Sometimes, a voltage sensor is used to achieve high performance in sensorless vector control; however, a voltage sensor for voltage error correction requires a higher response than that of the sensor-less drive voltage sensor. Therefore, there is a difficulty to detect the average value of the pulsewidth modulation waveform without delay.

The stability of the field-oriented vector control system is maintained by the disturbance observer, because the pole positions of the proposed system are combined with the conventional field-oriented vector control system and the disturbance observer. When the stability of both the disturbance observer and the field-oriented vector control are ensured, the system is stable.

B. Compensation Term for V/f Control Method

The *V/f* control is very useful in practical applications. A sensor-less drive system requires a higher cost controller and is sensitive to the motor parameters, especially in the low-speed region. In addition, *V/f* control has robust characteristics for the motor parameters. It should be noted that practical *V/f* control systems have current sensors for protection and compensation of the voltage error.

Fig. 6 shows a block diagram of the proposed method applied to *V/f* control. With this control method, the *d*-axis no longer

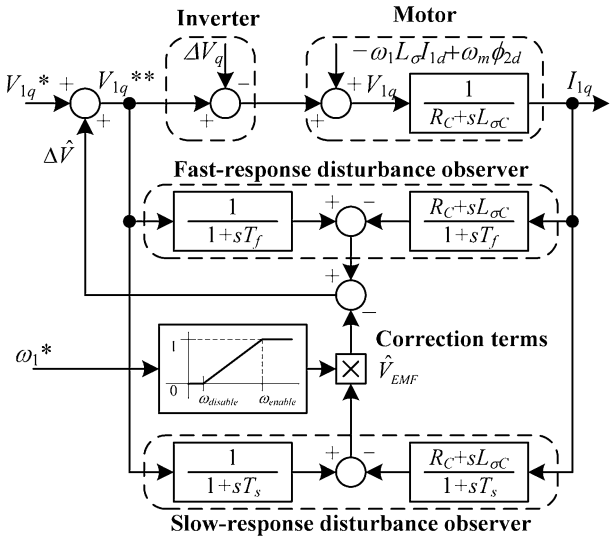

Fig. 6. Block diagram of voltage error correction method, using *V/f* control.

corresponds to the direction of the secondary flux vector. Therefore, the proposed disturbance observer is attached only to the *q*-axis, because the voltage error mainly appears in the *q*-axis with *V/f* control. On the other hand, an ACR is applied to the *d*-axis in order to maintain the excitation current. The ACR on the *d*-axis also improves the stability of the controller. In order to stabilize the system, K_{ACR} should be set as high as possible; however, the maximum value of K_{ACR} is limited by the delay time of the feedback loop in a practical system.

The cross term is calculated from the leakage inductance, *d*-axis current, and primary angular frequency. It should be noted that the cross term compensation is disabled in the low-speed region, because the rotation frame of the controller mismatches that of the motor.

The speed EMF term $\hat{V}_{\mathrm{EMF}}$ is also difficult to correct using the speed ω_m, because the *V/f* control does not have the motor speed information. The motor speed variation depends on a mechanical time constant, and the mechanical time constant of the motor is generally much longer than the electric time constant of the motor. The current distortion due to the voltage error is changed by the electric time constant, and the speed EMF has different frequency components to the voltage error. Therefore, a slow-response observer is designed to detect the speed EMF, and a fast-response observer is designed to detect the voltage error.

It is important to analyze a stability of the disturbance observer; however, the *V/f* control method is difficult to separate the *d*- and *q*-axis components in actual axes. Therefore, the stability of the proposed system was analyzed using a bode diagram and a root locus in the complex plane. The analyses conditions used the parameters of a general purpose 750-W induction motor under constant speed, in addition to those given in Table I.

Fig. 7(a) shows the bode diagram of the transfer function from the voltage error ΔV_q to the motor voltage V_{1q}. The bode diagram of the transfer function represents as a band eliminate filter. The gain indicates a negative value in the operation frequency from 1 to 50 Hz, which means that the voltage error does not appear in the motor terminal voltage because the gain of the transfer function becomes smaller though the phase property varies widely. On the other hand, the gain and phase are almost zero when located at outside of the operation range. When the controller parameters varied to half or double of the motor parameter, detail of the frequency response is slightly varied. However, the overall property of the frequency response is not changed; therefore, the affection of the motor parameter variation is negligible.

TABLE I
ANALYSIS CONDITIONS

Parameter	Value	Parameter	Value
Primary resistance R_1	2.78 Ω	Fast-response disturbance observer time constant T_f	1 ms
Secondary resistance R_2	2.44 Ω	Slow-response disturbance observer time constant T_s	500 ms
Leakage inductance L_σ	11.0 mH		

Fig. 7(b) shows the bode diagram of the transfer function from the command voltage V_{1q}^* to the motor voltage V_{1q}. When the controller parameters are same to the motor parameters, the gain and the phase is zero in all frequency range. The variation of motor resistance *R* makes phase shift in the operation frequency. On the other hand, the variation of motor inductance L_σ makes phase shift in the higher frequency range of the operation frequency.

Fig. 8(a) shows the root loci under the condition that $T_f = 1$ ms, $T_s = 100$ ms, $K_{\mathrm{ACR}} = 0.5$, and $\omega_1 = \omega_m = 0.65$ p.u. State equation (8), which is shown at the bottom of the next page, gives the root loci of proposed system. This system has six roots, because it is a sixth-order system. The positions of roots No. 1–4 in Fig. 8(a) indicate sufficient stability, because they are dispersed on the real axis in an area that is negatively distant from the imaginary axis. However, the remaining roots, Nos. 5 and 6, are located nearest to the imaginary axis. Therefore, the stability of the proposed system can be discussed based on root No. 5.

Fig. 8(b) shows the root No. 5 loci with variations in K_{ACR}, T_f, and T_s. Each of the parameters is varied $\pm 20\%$ from each of the given values. In order to stabilize the system, the roots should be located in the area negatively distant from the imaginary axis, in addition to minimizing the imaginary part. Thus, T_f and T_s are set to slower values, and K_{ACR} is set to a higher value in order to stabilize the system. It should be noted that a slow T_f avoids voltage error correction, and a slow T_s deteriorates the acceleration performance due to the back EMF. In contrast, K_{ACR} should be set as high as possible for stabilization, with consideration of the time delay of the feedback loop. As a result, the parameters should be designed according to the following terms.

1) T_f is set as fast as possible for the controller.
2) T_s is set to faster than the mechanical time constant.
3) K_{ACR} is then adjusted for the stability of the system.

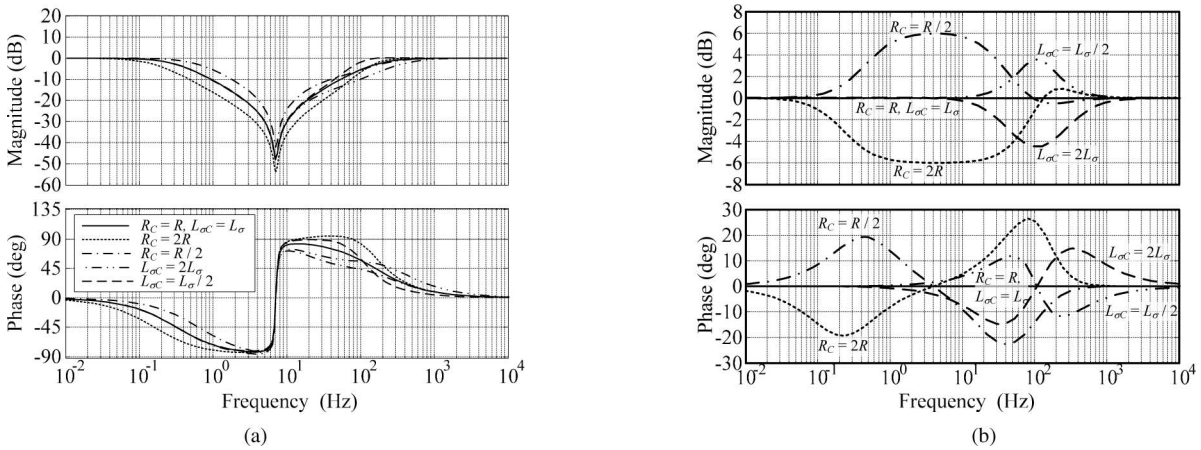

Fig. 7. Bode diagram of the proposed *V/f* control system. (a) Bode diagram of the transfer function from ΔV_q to V_{1q}. (b) Bode diagram of the transfer function from V_{1q}^* to V_{1q}.

IV. Experimental Result

A. Evaluation of the Proposed Voltage Error Compensation Method for Each Motor Control

Fig. 9 shows control block diagrams for the various control methods of the experimental system. Fig. 9(a) shows a block diagram for a 2.2 kW motor controlled using field-oriented vector control to maintain constant speed. Where T_d: dead-time period is 3 μs, f_s: switching frequency is 10 kHz, $V_{\rm dc}$: dc-link voltage is 300 V, sampling frequency is 10 kHz, ACR gain is 1 p.u., ACR time constant is 1 ms. Fig. 9(b) is based on reference [10], and it shows an experimental system composed of a general purpose induction motor and an inverter, where the motor is controlled using sensor-less vector control to maintain constant speed. Where T_d: dead-time period is 3 μs, f_s: switching frequency is 20 kHz, $V_{\rm dc}$: dc-link voltage is 300 V, sampling frequency is 10 kHz, ACR gain is 1 p.u., ACR time constant is 3 ms. This method estimates the motor speed from the speed EMF, which is calculated using voltage–current differential equation of the motor. The rotating frame of the controller corresponds with that of the motor by controlling the *d*-axis induced voltage. Fig. 9(c) shows a block diagram for the experimental system of a 750 W motor controlled using *V/f* control to maintain a constant primary frequency. Where T_d: dead-time period is 3 μs, f_s: switching frequency is 20 kHz, $V_{\rm dc}$: dc-link voltage is 300 V, sampling frequency is 10 kHz, $K_{\rm ACR}$: ACR gain is 2 p.u. In Fig. 9(c), the boost voltage is calculated using (9).

$$v_{\rm boost} = R_1 i_{1q} \left(1 - \frac{\omega_1^*}{\omega_n}\right). \tag{9}$$

Fig. 10 shows waveforms of the *d*-axis, *q*-axis, and *u*-phase current under conditions where the motor speed is 750 r/min with the rated load torque (1.0 p.u.) using field-oriented vector

$$
s\begin{bmatrix} i_d \\ i_q \\ \phi_{2d} \\ \phi_{2q} \\ \hat{V}_{\rm dist} \\ \hat{V}_{\rm emf} \end{bmatrix} =
\begin{bmatrix}
-\frac{K_{\rm ACR}}{L_\sigma} - \frac{R_1+R_2}{L_\sigma} & \omega_1 & \frac{R_2}{L_m L_\sigma} & \frac{\omega_{re}}{L_\sigma} & 0 & 0 \\
-\omega_1 & -\frac{R_1+R_2}{L_\sigma} & -\frac{\omega_{re}}{L_\sigma} & \frac{R_2}{L_m L_\sigma} & \frac{1}{L_\sigma} & -\frac{1}{L_\sigma} \\
R_2 & 0 & -\frac{R_2}{L_m} & (\omega_1 - \omega_{re}) & 0 & 0 \\
0 & R_2 & -(\omega_1 - \omega_{re}) & -\frac{R_2}{L_m} & 0 & 0 \\
\frac{L_{\sigma C}\omega_1}{T_f} & \frac{L_{\sigma C}}{L_\sigma}\frac{R_1+R_2}{T_f} - \frac{R_{1C}+R_{2C}}{T_f} & \frac{L_{\sigma C}}{L_\sigma}\frac{\omega_{re}}{T_f} & -\frac{L_{\sigma C}}{L_\sigma}\frac{R_2}{T_f L_m} & -\frac{L_{\sigma C}}{L_\sigma}\frac{1}{T_f} & -\frac{1}{T_f}\left(1 - \frac{L_{\sigma C}}{L_\sigma}\right) \\
\frac{L_{\sigma C}\omega_1}{T_s} & \frac{L_{\sigma C}}{L_\sigma}\frac{R_1+R_2}{T_s} - \frac{R_{1C}+R_{2C}}{T_s} & \frac{L_{\sigma C}}{L_\sigma}\frac{\omega_{re}}{T_s} & -\frac{L_{\sigma C}}{L_\sigma}\frac{R_2}{T_s L_m} & \frac{1}{T_s}\left(1 - \frac{L_{\sigma C}}{L_\sigma}\right) & -\frac{1}{T_s}\left(2 - \frac{L_{\sigma C}}{L_\sigma}\right)
\end{bmatrix}
$$

$$
\times \begin{bmatrix} i_d \\ i_q \\ \phi_{2d} \\ \phi_{2q} \\ \hat{V}_{\rm dist} \\ \hat{V}_{\rm emf} \end{bmatrix} + \begin{bmatrix} \frac{K_{\rm ACR}}{L_\sigma} \\ 0 \\ 0 \\ 0 \\ 0 \\ 0 \end{bmatrix} I_{1d}^* + \begin{bmatrix} 0 \\ \frac{1}{L_\sigma} \\ 0 \\ 0 \\ \frac{1}{T_f}\left(1 - \frac{L_{\sigma C}}{L_\sigma}\right) \\ \frac{1}{T_s}\left(1 - \frac{L_{\sigma C}}{L_\sigma}\right) \end{bmatrix} V_q^* + \begin{bmatrix} 0 \\ -\frac{1}{L_\sigma} \\ 0 \\ 0 \\ \frac{L_{\sigma C}}{L_\sigma}\frac{1}{T_f} \\ \frac{L_{\sigma C}}{L_\sigma}\frac{1}{T_s} \end{bmatrix} \Delta V \tag{8}
$$

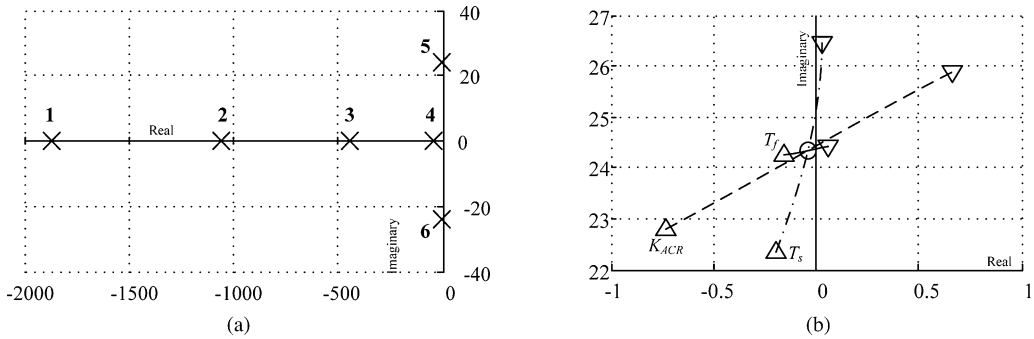

Fig. 8. Placement and loci of roots. O indicates no parameter variations, Δ indicates $+20\%$, and ∇ indicates -20%. The solid, dashed dot, and dashed lines represent the K_{ACR} current regulator gain and the T_f and T_s observer time-constant variations, respectively. (a) Placement of six roots. (b) Loci for the most vibratile root (No. 5).

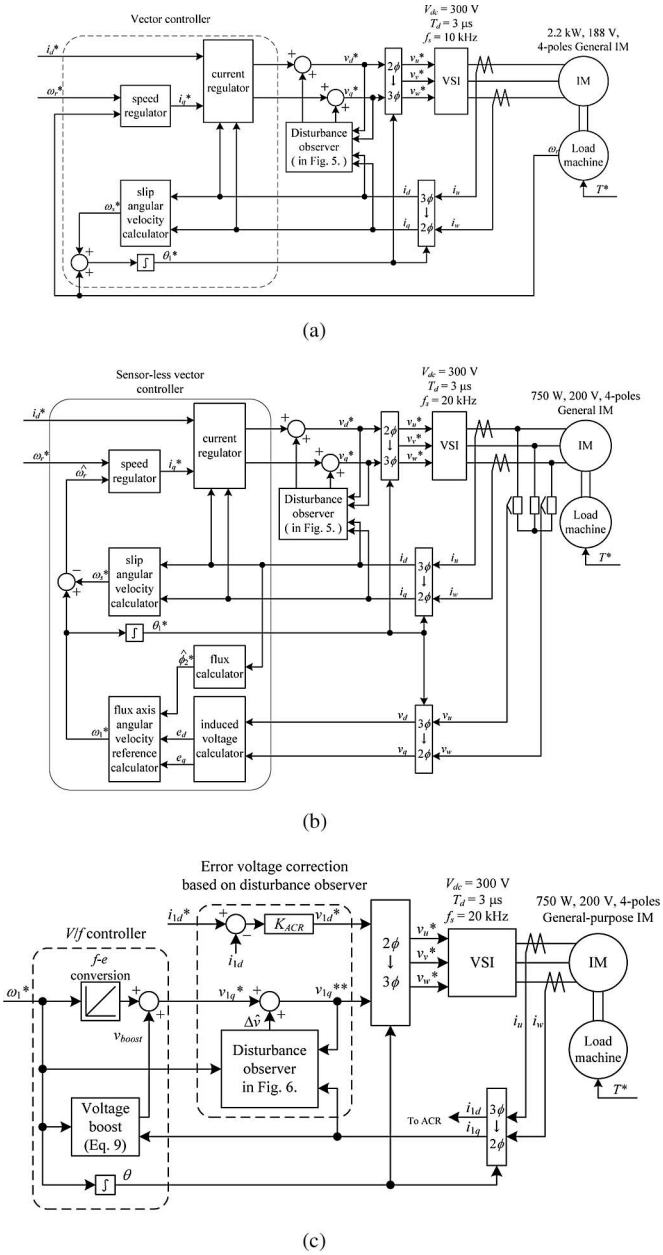

Fig. 9. Experimental systems for evaluation of correction performance. (a) Field-oriented vector control. (b) Sensor-less vector control. (c) *V/f* control.

control. The current distortion at the zero-crossing point of the *u*-phase current is also suppressed when using the voltage error correction method based on the disturbance observer. In order to evaluate performance of the proposed method, total harmonic distortion (THD) *k* is calculated as

$$k = \frac{\sqrt{I_2 + I_3 + \cdots + I_n}}{I_1} \tag{10}$$

where

I_1: RMS value of fundamental frequency of output current,

$I_2, I_3, \ldots I_n$: RMS value of *n*th-order harmonic of output current.

The THD of the current, as shown in Fig. 10(b), is 0.35%, which is a 1/3 reduction of that in Fig. 10(a). It is noted that the fundamental frequency component in the output current without the correction is reduced by the voltage error.

Fig. 10(c) shows the THD variation according to the motor speed. At middle- and high-speed region, frequency of the voltage error increases by increasing the frequency of the output voltage and current. Then THD will increases because the error correction performance of the PI controller is degraded when the frequency of the error voltage is increased. THD of the result using the conventional method is still high as the result of the PI controller because conventional method has errors in correction quantity and timing. However, THD of the result using proposed method is reduced below 1.0%. It should be noted that the voltage error correction using the disturbance observer can avoids problems, such as torque ripple or control precision, and improves the response of the acceleration, deceleration, and load variation.

Fig. 11 shows the waveforms of the motor speed, *d*-axis, *q*-axis, and *u*-phase current under conditions where the motor speed is 300 r/min with the rated load torque (1.0 p.u.) using sensor-less vector control. The experimental result shown in Fig. 11(a) is without voltage error correction and that in Fig. 11(b) is using the disturbance observer based on the voltage error correction method. In Fig. 11(a), the current distortion occurs at the zero crossing point of the *u*-phase current, because the voltage error is changing significantly at this point. In contrast, the distortion is almost corrected using the fast-response disturbance observer, as shown in Fig. 11(b).

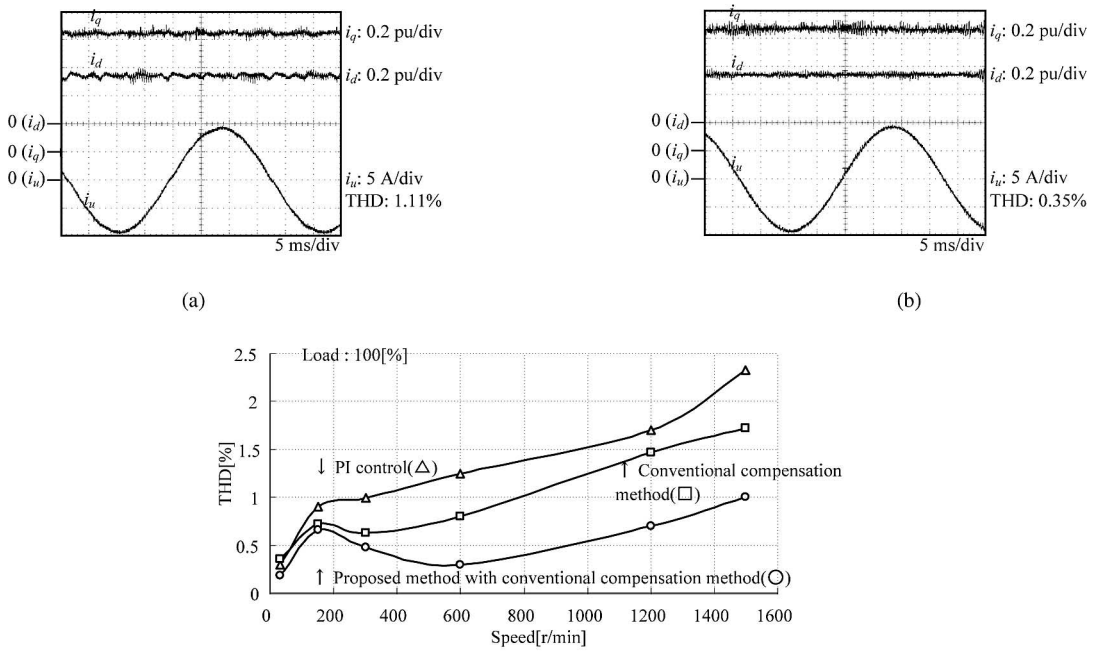

Fig. 10. Comparison of correction performance for a disturbance observer, using the field-oriented vector control method. (a) No correction method. (b) Correction method based on disturbance observer. (c) THD variation about motor speed.

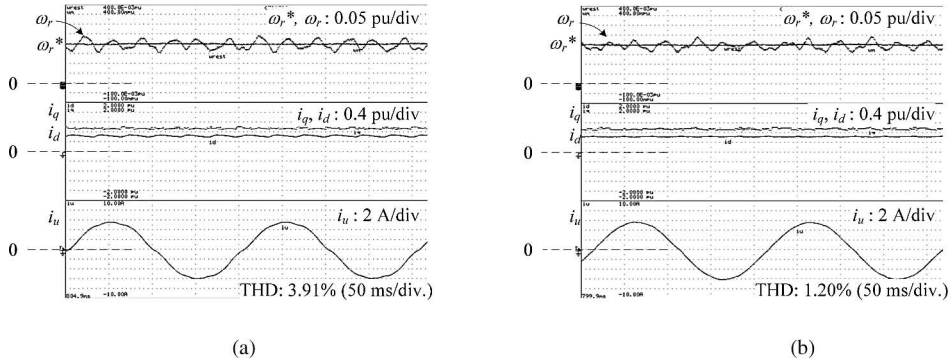

Fig. 11. Comparison of correction performance for a disturbance observer, using the sensor-less vector control method. (a) No correction method. (b) Correction method based on disturbance observer.

In addition, the THD of the current shown in Fig. 11(b) is 1.20%, which is a 1/3 reduction of that in Fig. 11(a).

Fig. 12 shows waveforms of the *d*-axis, *q*-axis, and *u*-phase current under conditions, where the primary side angular frequency is 1 Hz with no load torque using *V/f* control. The current distortion at the zero-crossing point of the *u*-phase current is also suppressed when using the voltage error correction method based on the disturbance observer. Accordingly, the THD of the current, as shown in Fig. 12(b), is 0.98%, which is a 1/9 reduction of that in Fig. 12(a).

It should be noted that the proposed method obtains the sinusoidal output voltage, which has no low order harmonics components because the output current is sinusoidal.

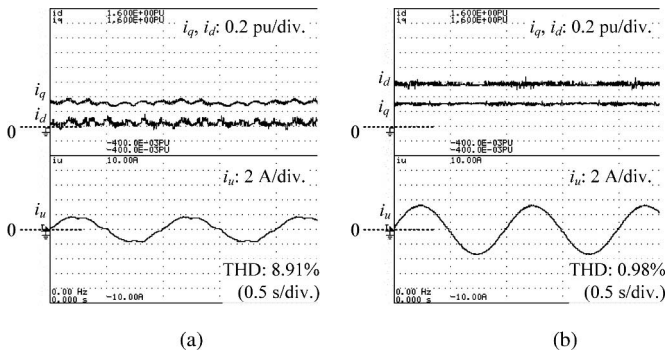

Fig. 12. Comparison of correction performance for a disturbance observer, using the *V/f* control method. (a) No correction method. (b) Correction method based on disturbance observer.

B. Sensitivity for Motor Parameter Variations

Fig. 13 shows the effect of R_C or $L_{\sigma C}$ parameter mismatches of on the THD, using the field-oriented vector control method. When R_C or $L_{\sigma C}$ was varied to R or L_σ multiplied or divided by two, the increase in the THD was less than 0.03 point. Therefore,

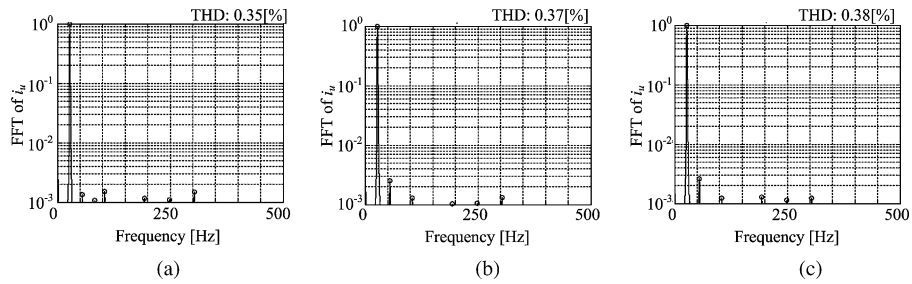

Fig. 13. Influence of parameter variations on vector control with the proposed compensation. (a) No parameter variations. (b) $R_c = 0.5R$, $L_{\sigma c} = 0.5L_\sigma$, (c) $R_c = 2R$, $L_{\sigma c} = 2L_\sigma$.

TABLE II
SUMMARY OF THE CURRENT THD FOR EACH CONTROL METHOD IN LOW-SPEED REGION

Control method	A: No correction	B: Correction method based on disturbance observer	B compared with A
Field-oriented vector	0.36%	0.19%	≈1/2
Sensor-less vector	3.91%	1.20%	≤1/3
V/f	8.91%	0.98%	≤1/9

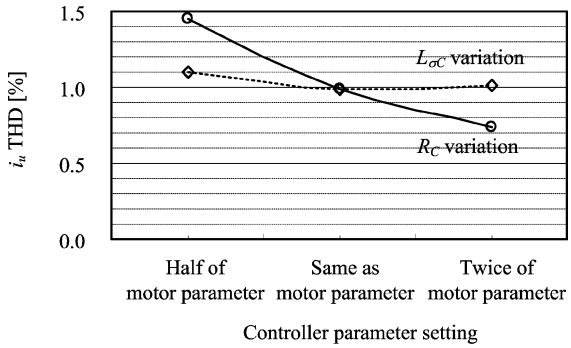

Fig. 14. THD variations for parameter mismatching with *V/f* control.

the proposed system has stable operation, even when there are parameter mismatches of R_C or $L_{\sigma C}$. It should be noted that the influence of the parameter variation on the sensor-less vector control is almost the same as that of the field-oriented control, because the sensor-less control has a flux estimator based on the field-oriented control.

Fig. 14 shows the effect of R_C or $L_{\sigma C}$ parameter mismatches on the THD, using the *V/f* control method. When R_C is smaller than *R*, the THD is increased. Similarly, when R_C is bigger than *R*, the THD is decreased. On the other hand, when the $L_{\sigma C}$ parameter is different to the actual L_σ, the THD is increased.

It is noted that the proposed method uses the current sensor to correct voltage error. Therefore, the gain and offset of the current sensor should be adjusted for each phase to achieve high performance in the adjustable speed drive system. The gain mismatching is the same as the parameter error of resistance R_C, because the gain of the transfer function from the actual current to the output voltage mentions resistance dimension. On the other hand, the offset and gain unbalance for each phase in the current sensor causes voltage commands and current ripple as same as other control methods.

C. Comparisons of Each Result

Table II shows a summary of the current THD for each control method in low-speed region less than 5 Hz. The correction method using the disturbance observer reduces the distortion of the current for all the control methods. In particular, THD of the current with *V/f* control was drastically reduced to 1/9, because the original *V/f* control method has no current regulators. As a result, the THD of the current with field-oriented vector control is decreased to 1/2, and the THD of the current with sensor-less method is decreased to 1/3. Therefore, the proposed voltage error correction method is effective for any of the control methods examined.

V. CONCLUSION

A disturbance observer was proposed for dead-time voltage error correction. Application of the proposed method was shown for field-oriented vector control and *V/f* control method. The proposed method is able to decrease the current distortion by 1/3 when using the field-oriented vector control method. When using the *V/f* control method, the proposed method is able to decrease the current distortion by 1/9. The proposed method is not dependent on the circuit topology; therefore, the proposed method can be used for voltage error correction with different circuit topologies, such as a matrix converter.

REFERENCES

[1] N. Urasaki, T. Senjyu, K. Uezato, and T. Funabashi, "An adaptive dead-time compensation strategy for voltage source inverter fed motor drives," *IEEE Trans. Power Electron.*, vol. 20, no. 5, pp. 1150–1160, Sep. 2005.
[2] T. Sukegawa, K. Kamiyama, K. Mizuno, T. Matsui, and T. Okuyama, "Fully digital, vector-controlled PWM VSI-fed AC drives with an inverter dead-time compensation strategy," *IEEE Trans. Ind. Appl.*, vol. 27, no. 3, pp. 552–559, May/Jun. 1991.
[3] J. W. Choi and S. K. Sul, "Inverter output voltage synthesis using novel dead time compensation," *IEEE Trans. Power Electron.*, vol. 11, no. 2, pp. 221–227, Mar. 1996.

[4] A. R. Munoz and T. A. Lipo, "On-line dead-time compensation technique for open-loop PWM-VSI drives," *IEEE Trans. Power Electron.*, vol. 14, no. 4, pp. 683–689, Jul. 1999.
[5] S.-G. Jeong and M.-H. Park, "The analysis and compensation of dead-time effects in PWM inverters," *IEEE Trans. Ind. Electron.*, vol. 38, no. 2, pp. 108–114, Apr. 1991.
[6] A. Cichowski and J. Nieznanski, "Self-tuning dead-time compensation method for voltage-source inverters," *IEEE Power Electron. Lett.*, vol. 3, no. 2, pp. 72–75, Jun. 2005.
[7] H. Zhao, Q. M. J. Wu, and A. Kawamura, "An accurate approach of nonlinearity compensation for VSI inverter output voltage," *IEEE Trans. Power Electron.*, vol. 19, no. 4, pp. 1029–1035, Jul. 2004.
[8] S. Kakizaki, M. Ito, T. Fukumoto, H. Hamane, and Y. Hayashi, "Measurement of parameters and the automatic measurement of an error voltage by dead time of an induction motor," in *IEEJ Annu. Meeting*, Mar. 2007, pp. 4–143.
[9] H. S. Kim, H. T. Moon, and M. J. Youn, "On-line dead-time compensation method using disturbance observer," *IEEE Trans. Power Electron.*, vol. 18, no. 6, pp. 1336–1345, Nov. 2003.
[10] H. Tajima, Y. Matsumoto, and H. Umida, "Speed sensorless vector control method for an industrial drive system," *Trans. IEEJ*, vol. 116-D, no. 11, pp. 1103–1109, Nov. 1996.
[11] L. Chen and F. Z. Peng, "Dead-time elimination for voltage source inverters," *IEEE Trans. Power Electron.*, vol. 23, no. 2, pp. 574–580, Mar. 2008.
[12] C. H. Choi, K. R. Cho, and J. K. Seok, "Inverter nonlinearity compensation in the presence of current measurement errors and switching device parameter uncertainties," *IEEE Trans. Power Electron.*, vol. 22, no. 2, pp. 576–583, Mar. 2007.
[13] V. Yousefzadeh and D. Maksimovic, "Sensorless optimization of dead times in DC–DC converters with synchronous rectifiers," *IEEE Trans. Power Electron.*, vol. 21, no. 4, pp. 994–1002, Jul. 2006.
[14] C. Attaianese, V. Nardi, and G. Tomasso, "A novel SVM strategy for VSI dead-time-effect reduction," *IEEE Trans. Ind. Appl.*, vol. 41, no. 6, pp. 1667–1674, Nov./Dec. 2005.
[15] J. A. Abu-Qahouq, H. Mao, H. J. Al-Atrash, and I. Batarseh, "Maximum efficiency point tracking (MEPT) method and digital dead time control implementation," *IEEE Trans. Power Electron.*, vol. 21, no. 5, pp. 1273–1281, Sep. 2006.
[16] W. Song and B. Lehman, "Dual-bridge DC–DC converter: A new topology characterized with no deadtime operation," *IEEE Trans. Power Electron.*, vol. 19, no. 1, pp. 94–103, Jan. 2004.
[17] X. Yuan, I. P. Brown, R. D. Lorenz, and A. Qui, "Observer based inverter disturbance compensation," presented at the IEEE Energy Conversion Congress and Exposition (ECCE 2009), San Jose, CA, Sep. pp. 20–24.
[18] Y. A.-R. I. Mohamed and E. F. El-Saadany, "Robust high bandwidth discrete-time predictive current control with predictive internal model: A unified approach for voltage-source PWM converters," *IEEE Trans. Power Electron.*, vol. 23, no. 1, pp. 126–136, Jan. 2008.

Tetsuma Hoshino (S'07) was born in Niigata, Japan, in 1983. He received the B.S. and M.S. degrees in electrical, electronics, and information engineering, in 2006 and 2008, respectively, from Nagaoka University of Technology, Nagaoka, Japan, where he has been working toward the Doctoral degree since 2008.

His current research interests include adjustable speed driving method and power converters.

Mr. Hoshino is a member of the Institute of Electrical Engineers of Japan.

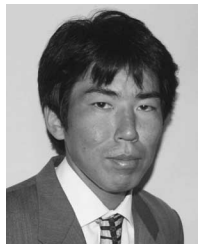

Jun-Ichi Itoh (M'01) was born in Tokyo, Japan, in 1972. He received the M.S. and Ph.D. degrees in electrical and electronic systems engineering from Nagaoka University of Technology, Nagaoka, Japan, in 1996, and 2000, respectively.

From 1996 to 2004, he was with Fuji Electric Corporate Research and Development Ltd., Tokyo, Japan. Since 2004, he has been with Nagaoka University of Technology, as an Associate Professor. His current research interests include matrix converters, dc/dc converters, power factor correction techniques, and motor drives.

Dr. Itoh is a member of the Institute of Electrical Engineers of Japan (IEEJ). He was the recipient of the IEEJ Academic Promotion Award (IEEJ Technical Development Award) in 2007.